Detection of Pseudomonas aeruginosa quorum sensing molecules at an electrified liquid|liquid micro-interface through facilitated proton transfer

Edward D. Burgoyne,[†] Andrés F. Molina-Osorio,[†] Reza Moshrefi,[‡] Rachel Shanahan,[§] Gerard P. McGlacken,[§] Talia Jane Stockmann,[‡,*] and Micheál D. Scanlon[†,*]

[†] The Bernal Institute and Department of Chemical Sciences, School of Natural Sciences, University of Limerick (UL), Limerick V94 T9PX, Ireland

[‡] Memorial University of Newfoundland, Chemistry Department, 283 Prince Philip Dr., St. John's, NL Canada A1B 3X7

[§] School of Chemistry and Analytical and Biological Chemistry Research Facility (ABCRF), University College Cork, College Road, Cork, Ireland

*Email: tstockmann@mun.ca (T.J.S)

*Email: micheal.scanlon@ul.ie (M.D.S)

Abstract

Miniaturization of electrochemical detection methods for point-of-care-devices is ideal for their integration and use within healthcare environments. Simultaneously, the prolific pathogenic bacteria Pseudomonas aeruginosa poses a serious health risk to patients with compromised immune systems. Recognizing these two factors, a proof-of-concept electrochemical method employing a micro-interface between water and oil (w/o) held at the tip of a pulled borosilicate glass capillary is presented. This method targets small molecules produced by P. aeruginosa colonies as signalling factors that control colony growth in a pseudo-multicellular process known as quorum sensing (QS). The QS molecules of interest are 4-hydroxy-2-heptylquinoline (HHQ) and 2-heptyl-3,4-dihydroxyquinoline (PQS, Pseudomonas quinolone signal). Hydrophobic HHQ and PQS molecules, dissolved in the oil phase, were observed electrochemically to facilitate proton transfer across the w/o interface. This interfacial complexation can be exploited as a facile electrochemical detection method for P. aeruginosa and is advantageous as it does not depend on the redox activity of HHQ/PQS. Interestingly, the limit-of-linearity is reached as [H+]≈[ligand]. Density functional theory calculations were performed to determine the proton affinities and gas-phase basicities of HHQ/PQS, as well as elucidate the likely site of stepwise protonation within each molecule.

Introduction

Persistent infectious bacteria form from the aggregation of the planktonic phenotype (so-called 'free-floating' bacteria), from which arises a biofilm phenotype that is protected by an alginate exopolysaccharide polymer matrix.[1-3] Biofilm-associated gram-negative bacteria, like *Pseudomonas aeruginosa*, pose a serious health risk to patients with compromised immune systems and suffers of cystic fibrosis (CF).[4, 5] In CF, *P. aeruginosa* colonize in the lungs disrupting respiratory function while increasing patient morbidity and mortality. These mucoid biofilm structures enhance antibiotic resistance through a variety of direct and indirect mechanisms. The formation of the biofilm is associated with the expression of quorum sensing (QS) molecules.[1, 2, 4, 6] QS small molecules are intercellular chemical signalling vectors that bacteria employ in a pseudo-multicellular fashion to regulate a host of behaviours with the aim of enhancing overall colony 'fitness'.[7] *P. aeruginosa* secretes multiple QS molecules (*e.g.*, 4-hydroxy-2-heptylquinoline, HHQ; 2-heptyl-3,4-dihydroxyquinoline, *i.e.*, pseudomonas quinolone signal, PQS; and pyocyanin) that also behave as virulence factors that directly inhibit the ciliary function of respiratory epithelial cells.[8] However, owing to their ability to permeate cell membranes these virulence factors have the potential to effect respiratory, urinary, and vascular function as well as presenting detrimental effects to the central nervous system.[9]

To confirm the presence of bacterial infections in CF patients, acquired sputum lung samples must be cultured for several days to isolate the bacterial strains present which is a highly costly and laborious process. Thus, there has been a push for the development of a number of rapid analytical methods for the detection of QS small molecules. Using rapid turn-around testing, patients would be diagnosed and receive treatment more quickly, thus reducing patient morbidity and mortality rates. This is of particular significance considering the increase in antibiotic resistant strains.[10-13] There is a plethora of quantitative and qualitative analytical methods for biofilm characterization including Coulter counter,[14] flow cytometry,[15] and scanning electron microscopy.[2] Recently, matrix assisted laser desorption/ionization mass spectroscopy (MALDI) employing ionic liquid matrices to enhance the detection of small molecules and coupled with dispersive liquid-liquid microextractions was successful in detecting PQS, HHQ, and pyocyanin in CF patient sputa.[5]

Meanwhile, the implementation of electroanalytical methods for high-throughput, rapid detection of QS small molecules by exploiting their redox activity has achieved success;[12, 16-42] *e.g.*, Buzid *et al*.[43] developed a boron-doped diamond electrode with nanomolar QS molecule detection levels. Moreover, microelectrodes have also been a means to characterize bacterial

growth and investigate intercellular communication through scanning electrochemical microscopy (SECM).[3, 17, 22, 39] Koley *et al*.[3] spatially mapped the concentration of pyocyanin above a cultured *P. aeruginosa* biofilm and discovered a concentration gradient in the reduced state pyocyanin that increased concomitantly as the SECM tip approached the biofilm. Several groups have implemented microelectrode arrays – often coupled with optical microscopies – to spatiotemporally monitor growth of the biofilm phenotype *in vitro*.[16, 32, 40] The spatiotemporal resolution of metabolite and QS molecules surrounding a bacterial colony is essential to understanding cell-to-cell communication at different growth stages of the biofilm. A complementary technique to a solid-solution electrode system is to use the electrified interface between two electrolytic solutions (ITIES); *e.g.*, the interface between water and oil (w/o) in which the Galvani potential difference ($\phi_w - \phi_o = \Delta_o^w \phi$) localized across the interface is mediated by two electrodes, one immersed in either phase.[44-47] Current changes across the ITIES are the result of charge transfer; *i.e.*, simple or facilitated/ligand assisted ion transfer as well as electron transfer.

Herein is presented an electrochemical method employing a micro-liquid-liquid interface (25 μm in diameter) between water and 1,2-dichloroethane for use in testing patient sputum extracts. The electrochemical signal originates from facilitated ion transfer across the liquid-liquid interface *via* PQS or HHQ interfacial coordination. As has been demonstrated, PQS behaves as ferric ion chelating agents that in-turn facilitate siderophore mediated iron uptake.[3, 48] Both molecules also behave as Lewis bases and have been shown to coordinate to alkali metals as well as protons.[42] Owing to their hydrophobicity these molecules are easily dissolved in organic solvents. Indeed, many bioassay protocols begin by first extracting QS molecules into an organic solution which is typically followed up by evaporation and redistribution steps.[49, 50] The proposed method would eliminate these steps and could be applied directly to the sputum extracts. Electroanalytical methods are further advantaged by their low cost, small laboratory/clinical footprint, and easy to use instrumentation relative to other analytical techniques like mass spectroscopy.

Using developed thermodynamic, analytical solutions to electrochemically induced liquid-liquid facilitated ion transfer,[51] HHQ and PQS interfacial proton coordination has been characterized at the micro-ITIES with proton:ligand stoichiometries of roughly 1:1. These complexes have been compared to density functional theory (DFT) calculations in order to determine the most reasonable protonation site on each molecule.

Experimental

All purchased chemicals were used as delivered without additional purification, unless indicated. 1,2-dichloroethane (DCE, ≥99.8%), lithium chloride (LiCl, ≥95%), tetraethylammonium chloride (TEACl, ≥98%), sodium 4-octylbenzenesulfonate dihydrate (NaOBSA, 98%), tetrabutylammonium perchlorate ($TBAClO_4$, ≥99%), bis(triphenylphosphoranylidene)ammonium chloride (BACl, 97%), and citric acid (≥99.5%) were purchased from Sigma-Aldrich. Lithium tetrakis(pentafluorophenyl)borate etherate ($Li(Et_2O)_nTB$), >99%) bought from Boulder Scientific was combined with BACl in a 1:1 ratio in 2:1, methanol:water to generate bis(triphenylphosphoranylidene)ammonium tetrakis(pentafluorophenyl)borate (BATB) by metathesis reaction. A white precipitate was obtained, filtered, and then recrystallized in acetone at ~4°C overnight (>99% yield by mass). Aqueous solutions were prepared with high purity water (>18.2 MΩ cm) using a Millipore MilliQ filtration system.

4-hydroxy-2-heptylquinoline (HHQ) and 2-heptyl-3,4-dihydroxyquinoline (PQS, Pseudomonas quinolone signal) were synthesized as previously described by McGlacken *et al.*[52] HHQ and PQS were deemed analytically pure based on NMR analysis. All spectra were consistent with that previously published.[53]

All electrochemical experiments were performed using a Metrohm potentiostat in a 3-electrode configuration using a modified pipette holder (HEKA Electroniks, Reutlingin, Germany), as described in detail elsewhere.[54, 55] The electrolytic cells employed are detailed in Scheme 1, where each vertical line represents a phase boundary, the double vertical line represents the polarisable ITIES held at the pipette tip, and with the aqueous phase filling the pipette. The potential was referenced to the transfer of ClO_4^-, taken to be –0.154 V,[56] unless otherwise noted.

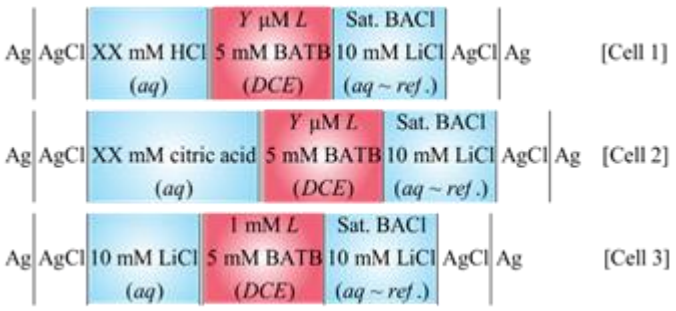

Scheme 1: Electrochemical Cells. In Cells 1, 2, and 3, *L* indicates the ligand (either HHQ or PQS) employed and *Y* indicates the ligand concentration (25, 50, or 100 μM). In Cells 1 and 2, the aqueous pH was adjusted with either HCl or citric acid, respectively.

Pulled borosilicate glass capillaries were fashioned into micropipettes in a method described previously.[54, 55, 57] The pore radius (~12.5 μm) was confirmed by tetraethylammonium (TEA^+) ion transfer cyclic voltammetry (CV) by varying the scan rate from 5-100 mV s^{-1} and comparing the linear progression of the ion peak transfer current to the Randles-Ševčík, equation (see the Electronic Supplementary Information, ESI, for details). DFT calculations were carried out using Compute Canada ACENet servers with pre- and postprocessing *via* GaussView software. Geometry optimization, structural, and electronic properties for HHQ and PQS were carried out at the Becke 3-parameter hybrid exchange and Lee-Yang-Parr (B3LYP) correlation DTF by using Pople's polarized double-ζ basis set, 6-31G(d,p),[58, 59] for all atoms with Gaussian 16.[60] Natural bond orbital analysis was applied to determine the atomic charges.

Results and Discussion

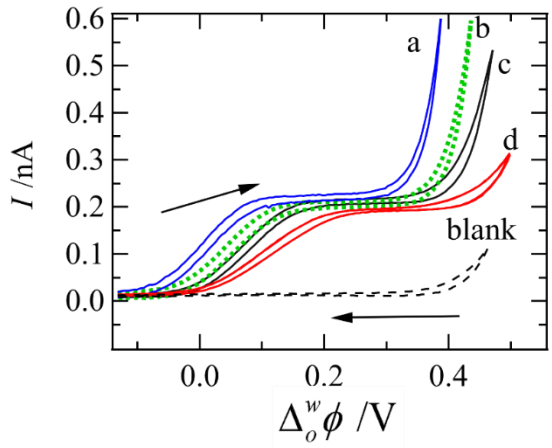

Figure 1: Cyclic voltammograms (CVs) recorded using Cell 1 with *L* = HHQ at 50 μM in the DCE phase, while the pH was adjusted using HCl from 2.5-4.0 (curves a-d). A scan rate of 25 mV s^{-1} was employed. The blank curve was obtained with no HHQ added to the DCE phase.

CVs obtained using Cell 1 with 50 μM of HHQ in the DCE phase while varying the pH using HCl in the aqueous phase have been plotted in Figure 1. Here HCl acts as both analyte

and supporting electrolyte. The Galvani potential difference between water and oil ($\phi_w - \phi_o = \Delta_o^w\phi$) spans the interface but occurs over only a few nanometers at most[61] and is the driving force for charge transfer. The dashed-black trace shows the response with no HHQ added to the DCE phase (blank curve) that is limited at positive and negative potentials by the transfer of protons and Cl^-, respectively, from the aqueous to organic phase (w→o).[56, 62] Once HHQ is introduced into the DCE phase, a steady-state wave was observed with half-wave potentials ($\Delta_o^w\phi_{1/2}$) that vary from –0.009 to 0.100 V as the pH of the aqueous phase is changed from 2.5 to 4.0. Ligands lower the overall Gibbs energy of ion transfer through complexation with metal ions or protons.[51, 54-56, 63-70] Owing to the asymmetric diffusion regime at a micropipette – linear inside and hemispherical outside[65] (see Figures S3 and S4 of the ESI) – and since $[H^+]>>[HHQ]$, it follows that the current signal would be diffusion limited by HHQ and generate the observed steady state current; therefore, this steady state wave is the facilitated transfer of protons by HHQ from w→o. Facilitated ion transfer has been studied extensively and several mechanisms have been elucidated;[51, 63, 64, 66-70] however, for simplicity and owing to the hydrophobic nature of HHQ, only transfer by interfacial complexation (TIC) or transfer followed by organic phase complexation (TOC) were considered. The analytical/thermodynamic solution for TIC and TOC are indistinguishable.[51] The overall reaction is described by,

$$m\mathrm{H}^+(aq) + nL(org) \rightleftharpoons \left[\mathrm{H}_m\text{-}L_n\right]^{m+}(org) \qquad [1]$$

where m and n are the H^+ and ligand (L) stoichiometries, respectively.

A facile analytical solution to the TIC/TOC mechanism was derived by Girault's group;[51] whereby, through a linear relationship two important thermodynamic coefficients can be obtained: (*i*) the overall complexation constant, β, and (*ii*) the H^+:ligand (m:n) stoichiometry. The overall solution for the $[H^+]>>[L]$ regime is,

$$\Delta_o^w\phi_{1/2,\mathrm{HL}_n^{m+}} \approx \Delta_o^w\phi_{H^+}^{o\prime} - \frac{RT}{mzF}ln\left(n\beta\left(\frac{c_L^*}{2}\right)^{n-1}\right) - \frac{RT}{zF}ln\left(c_{H^+}^*\right) \qquad [2]$$

where $\Delta_o^w\phi_{1/2,\mathrm{HL}_n^{m+}}$ is the half-wave potential of the H^+-ligand complex obtained from CV measurements; $\Delta_o^w\phi_{H^+}^{o'}$ is the formal ion transfer potential of H^+ taken to be 0.587 V;[56] c_L^* and $c_{\mathrm{H}^+}^*$ are the initial/bulk concentrations of the ligand and H^+, respectively; while R, T, z, and F have their usual significance. As has been shown,[65] if one assumes an n value of 1, then regardless of the value of m, equation 2 reduces to a linear relation,

$$-\frac{zF}{RT}\left(\Delta_o^w\phi_{1/2,\mathrm{HL}_n^{m+}} - \Delta_o^w\phi_{H^+}^{o'}\right) \approx \frac{1}{m}ln(\beta) + ln\left(c_{H^+}^*\right) \qquad [3]$$

With this in mind, the pH of the aqueous phase was varied using Cell 1 from 2.5-4.0 while [HHQ] was maintained in the DCE phase at either 25, 50, or 100 μM. Plots of $\delta = -\frac{zF}{RT}\left(\Delta_o^w\phi_{HL_n^+} - \Delta_o^w\phi_{H^+}^{o'}\right)$ *versus* $ln\left[c_{H^+}^*\right]$ obtained for each [HHQ] concentration are given in Figure 2 with panels A, B, and C corresponding to [HHQ] = 25, 50, and 100 μM, respectively. The red lines in Figure 2 are the product of linear regression analysis where the slope and *y*-intercept are the effective stoichiometry and lnβ, respectively. The results of the linear fitting are provided in Table 1 along with the Pearson's R value associated with each data set. There is good agreement between each of the three concentrations of HHQ. Since the slope of the linear fitting is ~1, the assumption that the H^+:HHQ stoichiometry of 1:1 employed in the generation of equation 3 is sound.

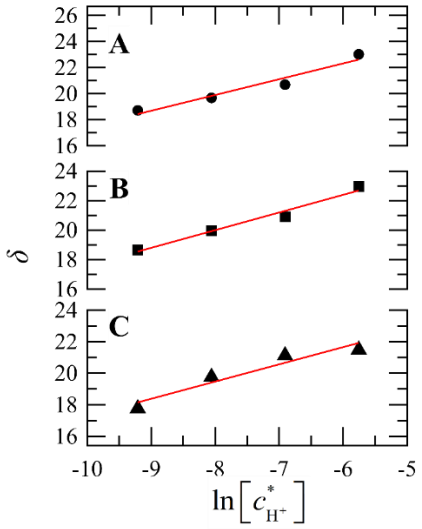

Figure 2: Plots of $\delta = -\frac{zF}{RT}\left(\Delta_o^w\phi_{HL_n^+,1/2} - \Delta_o^w\phi_{H^+}^{o'}\right)$ *versus* $ln\left[c_{H^+}^*\right]$ with $\Delta_o^w\phi_{HL_n^+,1/2}$ obtained from the ligand assisted half-wave potential of CVs as shown in Figure 1. Panels A, B, and C were computed from CVs using Cell 1 with *L* = HHQ and [HHQ] = 25, 50, and 100 μM, respectively. The red lines are the result of linear regression analysis.

Table 1: Linear regression data obtained from Figures 2 and 4 where c_L^* is the bulk/initial ligand concentration employed in the DCE phase, R is Pearson's R value, and lnβ represents the *y*-intercept.

Ligand (*L*)	c_L^*/μM	ln β	slope	R
HHQ	25	29.6	1.21	0.973
	50	29.6	1.20	0.988
	100	28.2	1.09	0.960
PQS	25	20.5	0.88	0.995
	50	20.9	0.91	0.987
	100	20.6	0.79	0.990

Figure S3 (see ESI) depicts CVs obtained using Cell 1 and 2 where the pH has been adjusted with either citric acid (curves a, b, and c) or HCl (curves d, e, and f) to pH 3.5, while 25 (curves a and d) and 50 μM (curves b and e) of HHQ were added in the DCE phase. While a small difference in the steady state current (i_{ss}) between the citric acid and HCl containing cells was observed, $\Delta_o^w\phi_{1/2}$ for HHQ assisted proton transfer does not vary by more than ±2 mV which is well within experimental error. For example, $\Delta_o^w\phi_{1/2}$ at 25 and 50 μM HHQ with citric acid was determined to be 0.082 and 0.068 V, while for Cell 1, with HCl $\Delta_o^w\phi_{1/2}$ was 0.080 and 0.068 V, respectively. Therefore, it can be concluded that for the proton sources tested, these sources do not influence H^+-HHQ binding.

Moving forward, the nature of PQS facilitated proton transfer was tested using Cell 1 with *L* = PQS. The pH in the aqueous phase was varied using HCl from 2.0-3.5 and the recorded CVs with [PQS] = 50 μM in DCE are presented in Figure 3. Without PQS added (blank trace) the CV is limited by H^+ and Cl^- transfer at positive and negative potentials, respectively. After addition of PQS a steady state curve was observed with $\Delta_o^w\phi_{1/2}$ varying from 0.145 to 0.227 V as the pH was changed from 2.0-3.5. Similar to the HHQ case, since [H^+] >> [PQS], then the facilitated ion transfer response should be diffusion limited by PQS in the DCE phase. This agrees well with the asymmetric pipette geometry which indicates a diffusion limited process in the DCE phase resembling redox responses at a recessed ultramicroelectrode. Therefore, the steady state wave observed in Figure 3 is facilitated proton transfer by PQS *via* equation 1. Owing to their similar chemical structure and hydrophobicity, H^+-PQS facilitated transfer likely proceeds through a TIC/TOC mechanism.

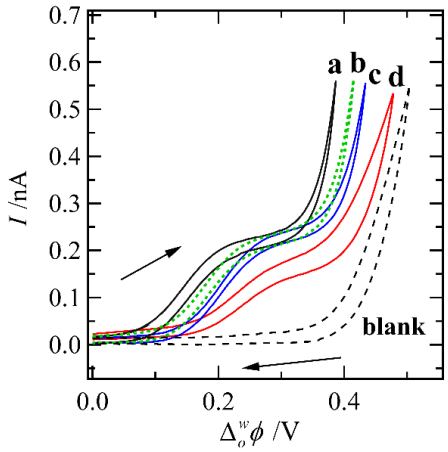

Figure 3: CVs recorded using Cell 1 with L = PQS at a concentration of 50 μM in DCE and aqueous pH varied using HCl from 2.0-3.5 (traces a-d). All other experimental parameters are the same as those described in Figure 1.

Using the $\Delta_o^w\phi_{1/2}$ obtained from the CVs in Figure 4, plots of $\delta = -\frac{zF}{RT}\left(\Delta_o^w\phi_{HL_n^+,1/2} - \Delta_o^w\phi_{H^+}^{o'}\right)$ *versus* $ln[c_{H^+}]$ were generated for 3 different PQS concentrations: 25, 50, and 100 μM for panels A, B, and C, respectively. The results of the linear regression analysis have been tabulated in Table 1. The slope of the linear fitting is ~1 indicating that the ligand and proton stoichiometry from equation 1 for PQS are 1:1 and agree well with each other.

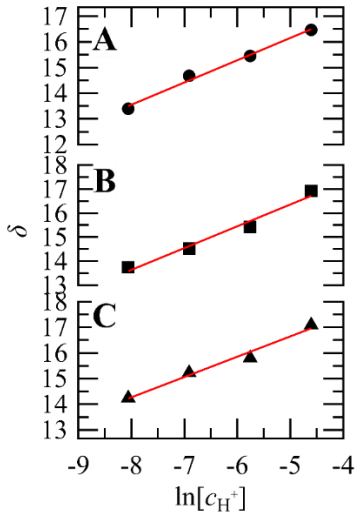

Figure 4: Plots of $\delta = -\frac{zF}{RT}\left(\Delta_o^w\phi_{HL_n^+,1/2} - \Delta_o^w\phi_{H^+}^{o'}\right)$ *versus* $ln[c_{H^+}]$ with L = PQS and $\Delta_o^w\phi_{HL_n^+,1/2}$ obtained from the experimental CVs shown in Figure 3. Panels A, B, and C were compiled from CVs using Cell 1 with [PQS] equal to 25, 50, and 100 μM, respectively.

The average overall complexation constants for equation 1 with 1:1 stoichiometry for H^+:HHQ and H^+:PQS are 4.4×10^{12} and 9.4×10^{8}, respectively. Since $K_a = 1/\beta$ these translate to pK_a's of 12.6 and 9.0, respectively and agree well with the first pK_a values estimated by Zhou *et al*.[53] using Marvin 6.8 software reported as 11.46 and 9.89, respectively. The pKa of HHQ is higher than that of PQS; this agrees well with our previous results at a large-ITIES.[42] The β values obtained for H^+-HHQ and H^+-PQS are similar to those obtained for phospholipid-proton interactions;[65] however, the n and β values differ from our previous study at a large-ITIES (stoichiometries of 3:1 and 2:1 for HHQ:H^+ and PQS:H^+, respectively)[42] due to the high concentrations of ligand employed in that work causing the protons to become saturated with ligand. Therefore, the overall complexation constants are not directly comparable between our previous work and this one.

Figure 5 contains examples of current signal *versus* ligand concentration plots (● traces) for HHQ (**A**) and PQS (**B**), at pH 2.5 as well as linear regression traces (solid, red lines). The dashed, black traces are based on the standard deviation with a 99.8% confidence interval as described in the ESI and by Skoog *et al*.[71] Signal detection limit based on 4 replicate blanks was 19.1 pA with a detection limit of 1.2 and 1.1 μM for HHQ and PQS, respectively. Signal *versus* concentration plots were generated for the other pH's (data not shown); R^2 values varied from 0.999 to 0.996 for HHQ and 0.999 to 0.976 for PQS. The measurement error increases concomitantly with ligand concentration. This is owing to the system transitioning from a $[H^+]>>$[ligand] to $[H^+]\approx$[ligand] state and from a ligand diffusion limited regime to one limited by protons. This in-turn results in the steady state current signal taking on a peak-shaped profile in the forward scan (see Figure S5 in the ESI).[44-47, 65] $[H^+]\approx$[ligand] therefore describes the limit of linearity for this method, particularly for HHQ. The error is relatively small and indicative of a sensitive electroanalytical technique that can be further improved by reducing the interfacial radius from micron to nano scale[72-75] or by employing micro/nano-arrays.[76-80]

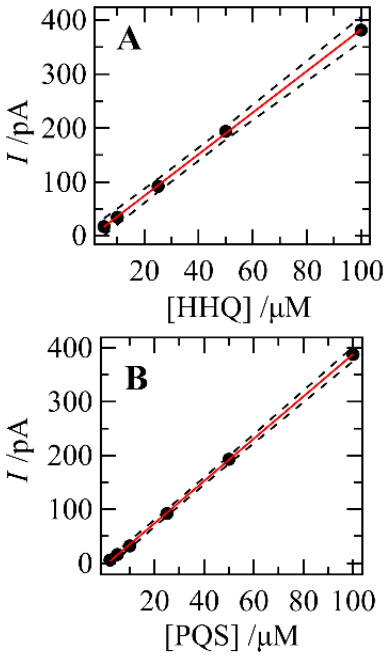

Figure 5: Current signal (pA) at pH 2.5 *versus* [HHQ] and [PQS] (μM, ● traces) plotted in panels **A** and **B**, respectively. The red, solid line is a product of linear regression analysis, while the dashed lines are the standard deviation of the *line-of-best-fit* based on a 99.8% confidence interval (for error analysis see ESI).

As was shown recently by Chai *et al.*[81] for *N*,*N*-dimethylaminobenzoic acid, determination of the protonation site can be complex and is impacted by electron-donating and -withdrawing substituents. Here, the phenol groups are known to possess inductive electron withdrawing character but simultaneously donate charge through resonance, while the ring embedded nitrogen typically has a high localized electron density *via* a lone pair of electrons. To investigate the protonation illustrated in Schemes 2 and 3 through site specific proton affinity and basicity, DFT computational analysis was employed; for computational ease and simplicity, only gas-phase reactions were considered.

As detailed in Scheme 2, HHQ and PQS were investigated for 2 and 3 protonation steps, respectively. The relative proton affinity (PA) and gas-phase basicity (GB) are defined as the negative enthalpy change (ΔH) and negative Gibbs energy change (ΔG), respectively, and their magnitudes have been presented relative to the initial HHQ or PQS molecule in Table 2.[82-84]

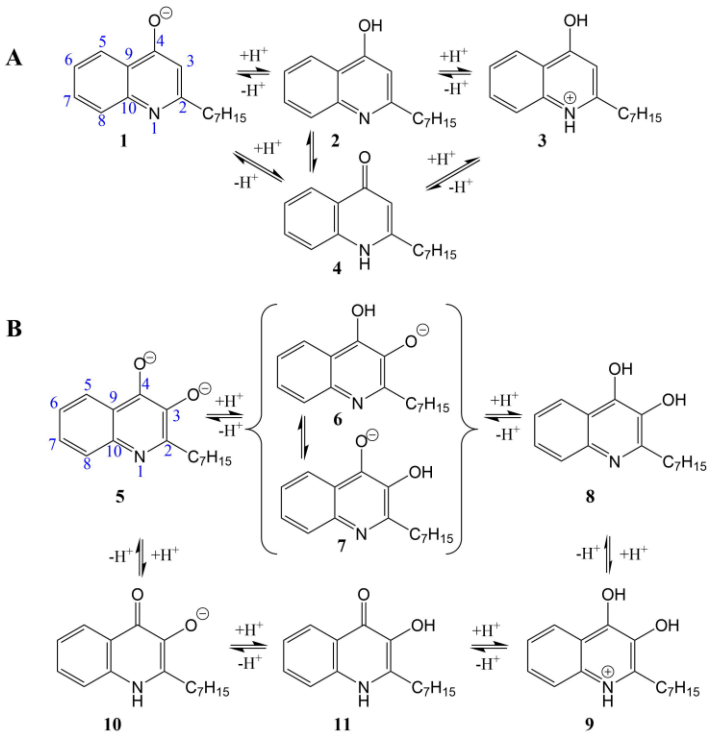

Scheme 2: HHQ (**A**) and PQS (**B**) protonation pathways through the quinoline and quinolone forms. The blue numbers around compound **1** and **5** indicate the numbering of positions.

Table 2: Proton affinities (PA) and gas-phase basicities (GB) for selected positions as indicated in Figure 6 on HHQ or PQS as determined through DFT computational analysis and relative to the initial molecule M in equation 4. C–O indicates protonation on oxygen. GB, PA, and Δ*S* have units of kJ mol^{-1}, kJ mol^{-1}, and J mol^{-1} K^{-1}, respectively.

	Protonation Step	Position	GB (kJ/mol)	PA (kJ/mol)	ΔS (J/molK)
HHQ	1 → 2	C(4)-O	1354.63	1385.53	0.294
	2 → 3	N(1)	970.88	1002.78	0.110
	1 → 4	N(1)	1367.15	1397.89	0.327
	4 → 3	C(4)-O	694.73	720.91	1.204
PQS	5 → 6	C(4)-O	1749.03	1773.00	1.626
	5 → 7	C(3)-O	1816.48	1842.76	1.182
	6 → 8	C(3)-O	1392.44	1422.15	0.332
	7 → 8	C(4)-O	1323.99	1352.40	0.775
	8 → 9	N(1)	961.67	995.06	–0.180
	5 → 10	N(1)	1734.77	1758.80	1.620

	10 → 11	C(3)-O	1438.35	1471.96	–0.229
	11 → 9	C(4)-O	929.01	959.46	0.387

Figure 6 illustrates the molecular electrostatic potential (MEP) maps for HHQ (**A**) and PQS (**B**) for the molecules given in Scheme 2 with the negative and positive electrostatic potential indicated in red and blue, respectively, while green is of intermediate potential. For species **1**, **4**, **5-7**, **10**, and **11** most electron density is localized on the oxygen(s), while **2** and **8** have electron density distributed on to an oxygen and the nitrogen; these are the likely sites for protonation.

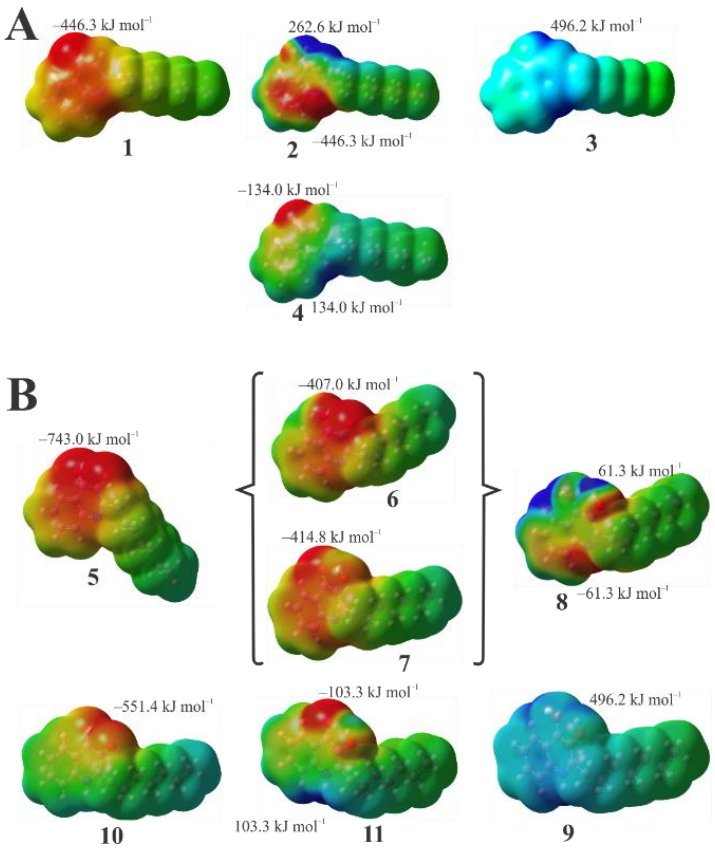

Figure 6: Molecular electrostatic potential (MEP) maps of HHQ (**A**) and PQS (**B**). Red and blue regions indicate areas of high positive and negative charge, respectively, with the potential values indicated inset. Bold numbers are the associated molecule numbers from Scheme 2.

As HHQ transitions along the quinoline path (**1** → **2** → **3**) the oxygen at C(4) is the first site of protonation (PA = 1385 kJ mol^{-1}), followed by N(1) (PA = 971 kJ mol^{-1}). For the quinolone path, protonation of N(1) is favourable (PA = 1398 kJ mol^{-1}), to give the quinolone isomer, and also emerges as a likely route, mirroring the existence of both isomeric forms.

For the PQS quinoline pathway, protonation at C(3)-O^- is favoured over the C(4)-O^- position; *i.e.*, **7** (PA = 1816 kJ mol^{-1}) is favoured over **6** (PA = 1749 kJ mol^{-1}). Thus, **7** was structurally optimized and used to determine the subsequent protonation step which follows at C(4)-O^-. Finally, N(1) protonation and the formation of **9** is associated with a PA of comparable value to N(1) in the formation of **3**. Similar to HHQ, the PQS quinolone pathway has a high PA (1759 kJ mol^{-1}) at N(1).

Aqueous and DCE solvent based DFT simulations are underway but are beyond the scope of the present work. The overall PA and GB values are in good agreement with similar organic molecules.[82-84]

Conclusions

The thermodynamics of HHQ/PQS facilitated proton transfer at an electrified micro-liquid-liquid interface have been investigated and revealed proton:ligand stoichiometries of 1:1 in the case of both QS molecules. Through established analytical solutions to facilitated ion transfer[51] the pKa's for HHQ and PQS were measured to be 12.6 and 9.0, respectively, and agree well with computed values.[53] The miniaturization of this analytical method along with these data provide a proof-of-concept biosensor for QS small molecule detection which could be applied to a clinical setting with 1 μM detection levels that could be improved by further reducing the ITIES size. Specification could be further enhanced by using a hydrophobic ionic liquid medium in place of the organic phase impregnated on a membrane and placed between the sputa sample and an acidified aqueous solution. While borosilicate glass capillaries have been used here, this could be replaced by a small disposable, single-use slide with a micropore on which a patient sample could be deposited and tested.

Meanwhile, DFT analysis revealed the likely protonation sites for HHQ and While calculated for gas-phase reactions, these data are likely to also be of interest to mass spectroscopists. Aqueous and DCE phase computational analysis of likely protonation sites are in progress but beyond the scope of the current work.

Conflict of Interest

There are no conflicts of interest to declare.

Acknowledgements

E.D.B. acknowledges funding received from an Irish Research Council Government of Ireland Postgraduate Scholarship Award (grant number GOIPG/2016/1217). This publication has emanated from research by M.D.S. and A.F.M.-O. supported by the European Research Council through a Starting Grant (agreement no. 716792) and in part by a research grant from Science Foundation Ireland (SFI) (grant number 13/SIRG/2137). G.M.G. and R.S. thank the Irish Research Council for funding. T.J.S is grateful to NSERC for funding with an NSERC Discovery Grant.

References

1. T. Bjarnsholt, M. Alhede, M. Alhede, S. R. Eickhardt-Sørensen, C. Moser, M. Kühl, P. Ø. Jensen and N. Høiby, *Trends Microbiol.*, 2013, **21**, 466-474.

2. L. C. Powell, M. F. Pritchard, E. L. Ferguson, K. A. Powell, S. U. Patel, P. D. Rye, S.-M. Sakellakou, N. J. Buurma, C. D. Brilliant, J. M. Copping, G. E. Menzies, P. D. Lewis, K. E. Hill and D. W. Thomas, *npj Biofilms and Microbiomes*, 2018, **4**, 13.

3. D. Koley, M. M. Ramsey, A. J. Bard and M. Whiteley, *Proc. Natl. Acad. Sci*, 2011, **108**, 19996-20001.

4. N. Høiby, O. Ciofu and T. Bjarnsholt, *Future Microbiol.*, 2010, **5**, 1663-1674.

5. J. Leipert, I. Bobis, S. Schubert, H. Fickenscher, M. Leippe and A. Tholey, *Anal. Bioanal. Chem.*, 2018, **410**, 4737-4748.

6. L. Fernández-Barat, O. Ciofu, K. N. Kragh, T. Pressler, U. Johansen, A. Motos, A. Torres and N. Hoiby, *J. Cyst. Fibros.*, 2017, **16**, 222-229.

7. M. Whiteley, S. P. Diggle and E. P. Greenberg, *Nature*, 2017, **551**, 313.

8. D. V. Vukomanovic, D. E. Zoutman, G. S. Marks, J. F. Brien, G. W. van Loon and K. Nakatsu, *J. Pharmacol. Toxicol. Methods*, 1996, **36**, 97-102.

9. S. Hall, C. McDermott, S. Anoopkumar-Dukie, A. J. McFarland, A. Forbes, A. V. Perkins, A. K. Davey, R. Chess-Williams, M. J. Kiefel, D. Arora and G. D. Grant, *Toxins*, 2016, **8**, 236.

10. E. Déziel, F. Lépine, S. Milot, J. He, M. N. Mindrinos, R. G. Tompkins and L. G. Rahme, *Proc. Natl. Acad. Sci*, 2004, **101**, 1339-1344.

11. C. T. Kåhrström, *Nat. Rev. Microbiol.*, 2013, **11**, 146.

12. O. Bukelman, N. Amara, R. Mashiach, P. Krief, M. M. Meijler and L. Alfonta, *Chem. Commun.*, 2009, DOI: 10.1039/B901125K, 2836-2838.

13. E. Tacconelli, E. Carrara, A. Savoldi, S. Harbarth, M. Mendelson, D. L. Monnet, C. Pulcini, G. Kahlmeter, J. Kluytmans, Y. Carmeli, M. Ouellette, K. Outterson, J. Patel, M. Cavaleri, E.

M. Cox, C. R. Houchens, M. L. Grayson, P. Hansen, N. Singh, U. Theuretzbacher, N. Magrini, A. O. Aboderin, S. S. Al-Abri, N. Awang Jalil, N. Benzonana, S. Bhattacharya, A. J. Brink, F. R. Burkert, O. Cars, G. Cornaglia, O. J. Dyar, A. W. Friedrich, A. C. Gales, S. Gandra, C. G. Giske, D. A. Goff, H. Goossens, T. Gottlieb, M. Guzman Blanco, W. Hryniewicz, D. Kattula, T. Jinks, S. S. Kanj, L. Kerr, M.-P. Kieny, Y. S. Kim, R. S. Kozlov, J. Labarca, R. Laxminarayan, K. Leder, L. Leibovici, G. Levy-Hara, J. Littman, S. Malhotra-Kumar, V. Manchanda, L. Moja, B. Ndoye, A. Pan, D. L. Paterson, M. Paul, H. Qiu, P. Ramon-Pardo, J. Rodríguez-Baño, M. Sanguinetti, S. Sengupta, M. Sharland, M. Si-Mehand, L. L. Silver, W. Song, M. Steinbakk, J. Thomsen, G. E. Thwaites, J. W. M. van der Meer, N. Van Kinh, S. Vega, M. V. Villegas, A. Wechsler-Fördös, H. F. L. Wertheim, E. Wesangula, N. Woodford, F. O. Yilmaz and A. Zorzet, *Lancet Infect. Dis.*, 2018, **18**, 318-327.

14. W. Zhang, E. S. McLamore, N. T. Garland, J. V. C. Leon and M. K. Banks, *J. Microbiol. Methods*, 2013, **94**, 367-374.

15. V. Ambriz-Aviña, J. A. Contreras-Garduño and M. Pedraza-Reyes, *BioMed Res. Int.*, 2014, **2014**, 461941.

16. O. Simoska, M. Sans, M. D. Fitzpatrick, C. M. Crittenden, L. S. Eberlin, J. B. Shear and K. J. Stevenson, *ACS Sensors*, 2019, **4**, 170-179.

17. H. J. Sismaet and E. D. Goluch, *Annu. Rev. Anal. Chem.*, 2018, **11**, 441-461.

18. C. R. Santiveri, H. J. Sismaet, M. Kimani and E. D. Goluch, *ChemistrySelect*, 2018, **3**, 2926-2930.

19. S. Li, Q. Mou, N. Feng and P. H. M. Leung, *Int. J. Electrochem. Sci.*, 2018, **13**, 3789-3798.

20. S. Kuss, H. M. A. Amin and R. G. Compton, *Chem. Asian J.*, 2018, **13**, 2758-2769.

21. R. Kataky and E. Knowles, *Curr. Opin. Electrochem.*, 2018, **12**, 121-128.

22. E. Darch Sophie and D. Koley, *Proc. Roy. Soc. A-Math Phys. Eng. Sci.*, 2018, **474**, 20180405.

23. A. Cernat, M. Tertis, I. Gandouzi, A. Bakhrouf, M. Suciu and C. Cristea, *Electrochem. Commun.*, 2018, **88**, 5-9.

24. Y. Yang, Y.-Y. Yu, Y.-Z. Wang, C.-L. Zhang, J.-X. Wang, Z. Fang, H. Lv, J.-J. Zhong and Y.-C. Yong, *Biosens. Bioelectron.*, 2017, **98**, 338-344.

25. H. J. Sismaet, A. J. Pinto and E. D. Goluch, *Biosens. Bioelectron.*, 2017, **97**, 65-69.

26. J. Oziat, M. Gougis, G. G. Malliaras and P. Mailley, *Electroanalysis*, 2017, **29**, 1332-1340.

27. J. Li, Y. Liu, E. Kim, J. C. March, W. E. Bentley and G. F. Payne, *Free Radical Biol. Med.*, 2017, **105**, 110-131.

28. J. Elliott, O. Simoska, S. Karasik, J. B. Shear and K. J. Stevenson, *Anal. Chem.*, 2017, **89**, 6285-6289.
29. A. Buzid, F. J. Reen, V. K. Langsi, E. Ó. Muimhneacháin, F. O'Gara, G. P. McGlacken, J. H. T. Luong and J. D. Glennon, *ChemElectroChem*, 2017, **4**, 533-541.
30. R. Burkitt and D. Sharp, *Electrochem. Commun.*, 2017, **78**, 43-46.
31. H. J. Sismaet, A. Banerjee, S. McNish, Y. Choi, M. Torralba, S. Lucas, A. Chan, V. K. Shanmugam and E. D. Goluch, *Wound Rep. Reg.*, 2016, **24**, 366-372.
32. D. L. Bellin, H. Sakhtah, Y. Zhang, A. Price-Whelan, L. E. P. Dietrich and K. L. Shepard, *Nat. Commun.*, 2016, **7**, 10535.
33. F. A. a. Alatraktchi, H. K. Johansen, S. Molin and W. E. Svendsen, *Nanomedicine*, 2016, **11**, 2185-2195.
34. J. Monzó, I. Insua, F. Fernandez-Trillo and P. Rodriguez, *Analyst*, 2015, **140**, 7116-7128.
35. T. A. Webster, H. J. Sismaet, J. L. Conte, I. p. J. Chan and E. D. Goluch, *Biosens. Bioelectron.*, 2014, **60**, 265-270.
36. H. J. Sismaet, T. A. Webster and E. D. Goluch, *Analyst*, 2014, **139**, 4241-4246.
37. F. Shang, E. Ó. Muimhneacháin, F. Jerry Reen, A. Buzid, F. O'Gara, J. H. T. Luong, J. D. Glennon and G. P. McGlacken, *Bioorg. Med. Chem. Lett.*, 2014, **24**, 4703-4707.
38. E. Kim, W. T. Leverage, Y. Liu, I. M. White, W. E. Bentley and G. F. Payne, *Analyst*, 2014, **139**, 32-43.
39. J. L. Connell, J. Kim, J. B. Shear, A. J. Bard and M. Whiteley, *Proc. Natl. Acad. Sci*, 2014, **111**, 18255-18260.
40. D. L. Bellin, H. Sakhtah, J. K. Rosenstein, P. M. Levine, J. Thimot, K. Emmett, L. E. P. Dietrich and K. L. Shepard, *Nat. Commun.*, 2014, **5**, 3256.
41. E. Kim, T. Gordonov, W. E. Bentley and G. F. Payne, *Anal. Chem.*, 2013, **85**, 2102-2108.
42. E. D. Burgoyne, T. J. Stockmann, A. F. Molina-Osorio, R. Shanahan, G. P. McGlacken and M. D. Scanlon, *J. Phys. Chem. C*, 2019, **123**, 24643-24650.
43. A. Buzid, F. Shang, F. J. Reen, E. Ó. Muimhneacháin, S. L. Clarke, L. Zhou, J. H. T. Luong, F. O'Gara, G. P. McGlacken and J. D. Glennon, *Sci. Reports*, 2016, **6**, 30001.
44. M. D. Scanlon, E. Smirnov, T. J. Stockmann and P. Peljo, *Chem. Rev.*, 2018, **118**, 3722-3751.
45. P. Peljo and H. H. Girault, in *Encyclopedia of Analytical Chemistry*, John Wiley & Sons, Ltd, 2012, DOI: 10.1002/9780470027318.a5306.pub2.
46. Z. Samec, J. Langmaier and T. Kakiuchi, *Pure Appl. Chem.*, 2009, **81**, 1473-1488.
47. S. Liu, Q. Li and Y. Shao, *Chem. Soc. Rev.*, 2011, **40**, 2236-2253.

48. S. P. Diggle, S. Matthijs, V. J. Wright, M. P. Fletcher, S. R. Chhabra, I. L. Lamont, X. Kong, R. C. Hider, P. Cornelis, M. Cámara and P. Williams, *Chem. Biol.*, 2007, **14**, 87-96.
49. M. P. Fletcher, S. P. Diggle, M. Cámara and P. Williams, *Nat. Protoc.*, 2007, **2**, 1254.
50. M. P. Fletcher, S. P. Diggle, S. A. Crusz, S. R. Chhabra, M. Cámara and P. Williams, *Environ. Microbiol.*, 2007, **9**, 2683-2693.
51. F. Reymond, G. Lagger, P.-A. Carrupt and H. H. Girault, *J. Electroanal. Chem.*, 1998, **451**, 59-76.
52. G. P. McGlacken, C. M. McSweeney, T. O'Brien, S. E. Lawrence, C. J. Elcoate, F. J. Reen and F. O'Gara, *Tetrahedron Lett.*, 2010, **51**, 5919-5921.
53. L. Zhou, F. J. Reen, F. O'Gara, C. M. McSweeney, S. L. Clarke, J. D. Glennon, J. H. T. Luong and G. P. McGlacken, *J. Chromatogr. A*, 2012, **1251**, 169-175.
54. T. J. Stockmann, A.-M. Montgomery and Z. Ding, *Can. J. Chem.*, 2012, **90**, 836-842.
55. T. J. Stockmann, Y. Lu, J. Zhang, H. H. Girault and Z. Ding, *Chem. Eur. J.*, 2011, **17**, 13206-13216.
56. M. Zhou, S. Gan, L. Zhong, X. Dong, J. Ulstrup, D. Han and L. Niu, *Phys. Chem. Chem. Phys.*, 2012, **14**, 3659-3668.
57. T. J. Stockmann, J. Zhang, A.-M. Montgomery and Z. Ding, *Anal. Chim. Acta*, 2014, **821**, 41-47.
58. P. C. Hariharan and J. A. Pople, *Theor. Chim. Acta.*, 1973, **28**, 213-222.
59. W. J. Hehre, R. Ditchfield and J. A. Pople, *J. Chem. Phys.*, 1972, **56**, 2257-2261.
60. M. J. Frisch, G. W. Trucks, H. B. Schlegel, G. E. Scuseria, M. A. Robb, J. R. Cheeseman, G. Scalmani, V. Barone, G. A. Petersson, H. Nakatsuji, X. Li, M. Caricato, A. V. Marenich, J. Bloino, B. G. Janesko, R. Gomperts, B. Mennucci, H. P. Hratchian, J. V. Ortiz, A. F. Izmaylov, J. L. Sonnenberg, Williams, F. Ding, F. Lipparini, F. Egidi, J. Goings, B. Peng, A. Petrone, T. Henderson, D. Ranasinghe, V. G. Zakrzewski, J. Gao, N. Rega, G. Zheng, W. Liang, M. Hada, M. Ehara, K. Toyota, R. Fukuda, J. Hasegawa, M. Ishida, T. Nakajima, Y. Honda, O. Kitao, H. Nakai, T. Vreven, K. Throssell, J. A. Montgomery Jr., J. E. Peralta, F. Ogliaro, M. J. Bearpark, J. J. Heyd, E. N. Brothers, K. N. Kudin, V. N. Staroverov, T. A. Keith, R. Kobayashi, J. Normand, K. Raghavachari, A. P. Rendell, J. C. Burant, S. S. Iyengar, J. Tomasi, M. Cossi, J. M. Millam, M. Klene, C. Adamo, R. Cammi, J. W. Ochterski, R. L. Martin, K. Morokuma, O. Farkas, J. B. Foresman and D. J. Fox, Gaussian 16 Rev. C.01, 2016
61. C. Wei, A. J. Bard and M. V. Mirkin, *J. Phys. Chem.*, 1995, **99**, 16033-16042.
62. T. J. Stockmann, A.-M. Montgomery and Z. Ding, *J. Electroanal. Chem.*, 2012, **684**, 6-12.
63. T. Shioya, S. Nishizawa and N. Teramae, *Langmuir*, 1999, **15**, 2575-2579.

64. T. Shioya, S. Nishizawa and N. Teramae, *Langmuir*, 1998, **14**, 4552-4558.

65. T. J. Stockmann, J.-M. Noel, A. Abou-Hassan, C. Combellas and F. Kanoufi, *J. Phys. Chem. C*, 2016, **120**, 11977–11983.

66. Á. Molina, E. Torralba, C. Serna and J. A. Ortuño, *J. Phys. Chem. A*, 2012, **116**, 6452-6464.

67. E. Torralba, A. Molina, C. Serna and J. A. Ortuno, *Int. J. Electrochem. Sci.*, 2012, **7**, 6771-6786.

68. Z. Samec, D. Homolka and V. Mareček, *J. Electroanal. Chem. Interfacial Electrochem.*, 1982, **135**, 265-283.

69. D. Homolka, K. Holub and V. Mareček, *J. Electroanal. Chem. Interfacial Electrochem.*, 1982, **138**, 29-36.

70. T. Kakiuchi and M. Senda, *J. Electroanal. Chem.*, 1991, **300**, 431-445.

71. D. A. Skoog, *Principles of instrumental analysis*, Fourth edition. Fort Worth : Saunders College Pub., [1992] ©1992, 1992.

72. Y.-L. Ying, Z. Ding, D. Zhan and Y.-T. Long, *Chem. Sci.*, 2017, **8**, 3338-3348.

73. M. D. Scanlon, J. Strutwolf, A. Blake, D. Iacopino, A. J. Quinn and D. W. M. Arrigan, *Anal. Chem.*, 2010, **82**, 6115-6123.

74. M. D. Scanlon and D. W. M. Arrigan, *Electroanalysis*, 2011, **23**, 1023-1028.

75. D. W. M. Arrigan and Y. Liu, *Annu. Rev. Anal. Chem.*, 2016, **9**, 145-161.

76. D. W. M. Arrigan and G. Herzog, *Curr. Opin. Electrochem.*, 2017, **1**, 66-72.

77. B. M. B. Felisilda, A. D. Payne and D. W. M. Arrigan, *Anal. Chem.*, 2018, **90**, 10256-10262.

78. R. Akter and D. W. M. Arrigan, *Anal. Chem.*, 2016, **88**, 11302-11305.

79. J. Strutwolf, M. D. Scanlon and D. W. M. Arrigan, *J. Electroanal. Chem.*, 2010, **641**, 7-13.

80. J. Strutwolf, M. D. Scanlon and D. W. M. Arrigan, *Analyst*, 2009, **134**, 148-158.

81. Y. Chai, G. Weng, S. Shen, C. Sun and Y. Pan, *J. Am. Soc. Mass. Spectrom.*, 2015, **26**, 668-676.

82. A. Moser, K. Range and D. M. York, *J Phys Chem B*, 2010, **114**, 13911-13921.

83. A. L. L. East, B. J. Smith and L. Radom, *J. Am. Chem. Soc.*, 1997, **119**, 9014-9020.

84. E. P. L. Hunter and S. G. Lias, *J. Phys. Chem. Ref. Data*, 1998, **27**, 413-656.